Title

Stem Cell–Derived Endochondral Cartilage Stimulates Bone Healing by Tissue Transformation

Journal

Journal of Bone and Mineral Research, 29(5)

ISSN

0884-0431

Authors

Bahney, Chelsea S
Hu, Diane P
Taylor, Aaron J
et al.

Publication Date

2014-05-01

DOI

10.1002/jbmr.2148

Peer reviewed

HHS Public Access

Author manuscript

J Bone Miner Res. Author manuscript; available in PMC 2016 March 22.

Published in final edited form as:

J Bone Miner Res. 2014 ; 29(5): 1269–1282. doi:10.1002/jbmr.2148.

Stem cell derived endochondral cartilage stimulates bone healing by tissue transformation

Chelsea S Bahney, PhD[1,2,*], **Diane P Hu, MD**[1], **Aaron J Taylor, BS**[1], **Federico Ferro, PhD**[1], **Hayley M Britz, MS**[3], **Benedikt Hallgrimsson, PhD**[3], **Brian Johnstone, PhD**[2], **Theodore Miclau, MD**[1], and **Ralph S Marcucio, PhD**[1]

[1]University of California, San Francisco (UCSF) & San Francisco General Hospital (SFGH), Orthopaedic Trauma Institute, 2550 23rd Street, Building 9, 3rd Floor, San Francisco, CA 94110

[2]Oregon Health & Science University, Department of Orthopaedics & Rehabilitation, OP31, 3181 SW Sam Jackson Road, Portland, OR 97239, Phone: (503) 494-9505, Fax: (503) 494-5050

[3]University of Calgary, Department of Cell Biology and Anatomy, McCaig Bone and Joint Institute, 3330 Hospital Drive, NW, Calgary, AB, Canada T2N 4N1, Tel: (403) 220-8632, Fax: (403) 210-3829

Abstract

Although bone has great capacity for repair, there are a number of clinical situations (fracture non-unions, spinal fusions, revision arthroplasty, segmental defects) in which auto- or allografts augment bone regeneration. Critical failures associated with current grafting treatments include osteonecrosis and limited integration between graft and host tissue. We speculated that the underlying problem with current bone grafting techniques is that they promote bone regeneration through direct osteogenesis. We hypothesized that using cartilage to promote endochondral bone regeneration would leverage normal developmental and repair sequences to produce a well-vascularized regenerate that integrates with the host tissue. In this study we use a translational murine model of a segmental tibia defect to test the clinical utility of bone regeneration from a cartilage graft. We further test the mechanism by which cartilage promotes bone regeneration using *in vivo* lineage tracing and *in vitro* culture experiments. Our data show that cartilage grafts support regeneration of a vascularized and integrated bone tissue *in vivo*, and subsequently propose a translational tissue engineering platform using chondrogenesis of MSCs. Interestingly, lineage tracing experiments show the regenerate was graft derived, suggesting transformation of the chondrocytes into bone. *In vitro* culture data shows that cartilage explants mineralize with the addition of BMP or by exposure to HUVEC conditioned medium, indicating that endothelial cells directly promote ossification. This study provides pre-clinical data for endochondral bone repair that has potential to significantly improve patient outcomes in a variety of musculoskeletal diseases and injuries. Further, in contrast to the dogmatic view that hypertrophic chondrocytes

[*]corresponding author: bahneyc@orthosurg.ucsf.edu or 415-206-5362.

Disclosures

There are no competing or conflicts of interest to report related to the work presented in this manuscript for any of the authors. Author contribution to the paper was as follows: study design: CSB, DPH, TM, RSM; study conduct and data collection: CSB, DPH, AJT, FF; Data interpretation: CSB, DPH, AJT, FF, BJ, TM, RSM; Drafting manuscript: CSB; Revising Manuscript: CSB, RM; Approval of final version of manuscript: CSB, DPH, AJT, FF, BJ, TM, RSM. CSB take responsibility for the integrity of the data.

undergo apoptosis prior to bone formation, our data suggest cartilage can transform into bone by activating the pluripotent transcription factor Oct4A. Together these data represent a paradigm shift describing the mechanism of endochondral bone repair and open the door for novel regenerative strategies based on improved biology.

Keywords

Molecular pathways; Remodeling; Orthopaedics; Bioengineering; Orthopaedics; Injury/Fracture Healing; Therapeutics; Chondrocytes and Cartilage Biology

Introduction

There is a significant unmet clinical need to develop improved strategies for promoting vascularized bone regeneration. The Global Burden of Disease 2010 report recently published in The Lancet determined musculoskeletal diseases to be the second greatest cause of disability worldwide (1), and in the United States the healthcare cost burden associated with trauma has surpassed that of cardiovascular disease (2). Bone grafting is an interventional technique used to restore structural integrity and promote bone repair in a diverse set of musculoskeletal conditions. Common indications for bone grafting include: traumatic injuries sustained in motor vehicle accidents and war, fracture non-unions, spinal fusions, osteotomies from tumor resection, arthrodesis, and around joint replacements. Bone is the second most commonly transplanted tissue (behind blood) with an estimated 1.6 million grafting procedures performed annually (3). The gold standard grafting technique remains transplantation of autologous bone. However, autologous grafting is associated with a number of clinical shortcomings, including: limited availability of donor tissue, donor site morbidity, and increased potential for additional surgeries. Allografted bone, bone graft substitutes, and bone tissue engineering represent techniques to address inherent limitations of autografts. Despite recent progress in these technologies, poor graft integration and osteonecrosis remain problematic (4), and clinical failure associated with bone allografts are estimated to be between 16–35% (5).

In this study we explore the idea of using cartilage tissue as a method to stimulate bone repair through endochondral ossification. We speculated that an underlying problem with current bone grafting technologies is that they promote bone regeneration through direct osteogenesis. However, long bone formation and fracture healing typically proceed via a cartilage intermediate, suggesting that an endochondral tissue therapy may be a more clinically and biologically appropriate treatment. Cartilage is physiologically adapted to function well under avascular conditions, and hypertrophic chondrocytes within endochondral cartilage stimulate vasculogenesis. These inherent biological features of cartilage propound that it may be a better therapeutic strategy for bone regeneration. We hypothesized that by promoting endochondral ossification using cartilage tissue grafts we could address the clinical shortcomings of current technologies to produce a well-vascularized bone regenerate that integrates with the host tissue.

The molecular details of endochondral ossification are understood predominantly in the context of long bone development (6). First, mesenchymal cells condense and undergo

chondrogenesis to form a cartilaginous model of the future bone. Chondrocytes within this anlagen organize into morphologically and functionally distinct domains that correspond to their maturation state (resting, proliferating, hypertrophic) and allow for longitudinal growth. Hypertrophic chondrocytes are believed to be the terminal maturation state of the chondrocyte. Upon maturation, chondrocytes undergo apoptosis, the cartilage matrix is degraded and replaced by the marrow cavity, and bone forms in the adjacent perichondrium to form the diaphysis of the long bones (7). Hypertrophic chondrocytes are distinguished by their enlarged round shape, and expression of type X collagen, matrix metalloproteinase-13 (MMP-13), and vascular endothelial growth factor (VEGF). These proteins are essential in recruiting osteoblast precursors from the surrounding tissue, promoting vascularization, and mineralization of the extracellular matrix. Repair of non-stabilized fractures also occurs through a cartilage intermediate (8), in a process that is presumed to follow endochondral ossification during skeletogenesis. In a murine tibia fracture an avascular cartilage callus (~day 5) precedes vascular invasion, mineralization and remodeling into bone (~days 10–28).

Despite many similarities between endochondral ossification during development and repair, the therapeutic application of cartilage tissue for promoting bone regeneration has not been established experimentally. The overall goal of this study was to utilize a translational murine model of segmental bone defects to validate cartilage grafts as a potential treatment strategy for bone repair. Further, by studying the molecular details during healing we aimed to understand how the cartilage graft (donor tissue) and host tissue contribute to the repair process. An accurate assessment of how cartilage grafts facilitate bone regeneration is a necessary foundation for building an effective clinical strategy to promote endochondral repair. Design of scaffold material, cell/tissue source, and bioactive reagents will all depend on the fate of the chondrocytes, source of osteoblasts, and role of the vasculature during the repair process.

The data presented in this study demonstrate that cartilage grafts produce a well-vascularized and integrated bone regenerate in murine segmental tibial defects, implying that cartilage may be a better therapeutic effector for modulating bone regeneration than bone itself. Further, genetic labeling of the donor and host tissue revealed that the bone regenerate is donor/cartilage derived, suggesting that chondrocytes may directly transform into osteoblasts. This mechanism of repair significantly contrasts endochondral ossification during long bone development, requiring that we re-evaluate the mechanisms of endochondral repair in order to improve bone regeneration strategies.

Materials & Methods

Fractures

All animal studies were approved by the UCSF IACUC. Adult, male mice (10–14 weeks) were anesthetized and a standardized, closed non-stable fracture was made in the mid-diaphysis of the tibia using a custom-built apparatus designed to deliver a reproducible three-point bending fracture by controlling the weight (460 g) and distance (14 cm) of the force. Fractures were not stabilized to promote endochondral repair and animals were provided with Buprenex as needed.

Tissue Grafts into the Tibia Defect Model

A 2 mm segmental defects created by an osteotomy in the mid-tibial diaphysis of immunocompromised mice (SCID Beige Mice, Charles River #250) (Figure 1C). One of four different tissue grafts was transplanted into the defect: cartilage grafts, living cortical bone grafts ("isograft"), devitalized cortical bone grafts ("allografts"), or stem cell-derived cartilage pellets (See below). As a control the critical sized defect remained empty. Cartilage grafts were isolated from the central portion of a day 7 fracture callus (Figure 1B) *ex vivo* by using a microscope to dissect out the cartilage and remove all non-cartilaginous adherent tissues and the perichondrium. Isografts were created by simply replacing the osteotomized bone into the defect, and allografts were created by washing osteotomized bone in 70% EtOH and freezing at −80°C as previously described (9–11). A 8.0 suture was used to secure graft in place by closing the muscle. Tibiae were externally stabilized with a customized circular fixator consisting of two 2 cm circular rings held concentrically by three threaded rods (Figure 1C). This device provides rigid fixation; this model/method has been extensively described previously (12, 13). Animals were survived for 1–6 weeks, with a minimum of 5 animals analyzed histologically at each time point and 8 animals analyzed at 4 weeks by μCT and biomechanical testing.

μCT and Biomechanical Testing

A Scanco Medical AG μCT was used to scan both the grafting area and fracture callus. Samples were rotated through 360° and the X-ray settings were standardized to 70 kV and 114 μA, with an exposure time of 0.14 seconds per frame to yield a nominal resolution of 10.5 μm. A 0.5 mm thick aluminum filter was employed to minimize beam-hardening artifacts. Scan time for each sample was approximately 50 minutes. Bone mineral density was analyzed from 200 slices within the integration site or fracture callus, using a custom made script. Briefly, bone mineral density (BMD) was measured by normalizing mineral content from the X-ray attenuation by bone volume. Integration was scored (0 = no integration, or 1= integration) based on μCT images to indicate incidence of integration. After scanning, the tibiae were subjected to three-point bending using an ElectroForce 3200 testing machine (Bose Corp., Eden Prairie, USA) to measure the integration strength. Only grafts that had integrated both proximally and distally were tested mechanically. Tibiae were placed on their lateral surface on the lower supports of the bending jig in supports located under the tibia-fibula junction and the tibial crest. A preload of 1 N was applied from above at the midpoint between the two lower supports to stabilize the bone. The load applied to the bone was measured by a 450 N load cell at a displacement rate of 2 mm/min. A load-displacement curve was generated for each bone and used to determine ultimate load. Statistical differences for integration success was tested using a pairwise comparison between cartilage, isograft and allograft and Fisher Exact Test. BMD and ultimate failure data were compared using an ANOVA followed by Tukeys HSD pairwise comparison. P-values less that 0.05 were considered significant.

Bone Tissue Embedding and Histology

Tibiae from euthanized mice or *in vitro* cartilage grafts were collected and fixed in freshly made 4% paraformaldehyde (PFA, pH 7.2–7.4) for 24 hours at 4°C. Tibiae were decalcified

in 19% EDTA (pH 7.4) for 14 days at 4°C and then processed for paraffin or frozen histology. Histology staining to visualize bone and cartilage tissues was completed: Modified Milligan's Trichrome (bone = blue), Safranin O/fast green (cartilage = red), or Hall and Brunt Quadruple stain (HBQ, bone = red, cartilage = blue).

Immunohistochemistry on Bone Tissue

X-gal staining was used to detect for β-galactosidase on frozen sections post-fixed in 0.2% glutaraldehyde for 15 min, and then exposed to x-gal staining solution overnight at 37°C. Immunohistochemistry (IHC) for eGFP (Invitrogen A10259) was performed by treating sections with 0.3% Triton X (15 min), 0.05% trypsin (20 min, 37°C), 10mM sodium citrate buffer (30 min, 100°C), 3% H_2O_2 in methanol (30 min), and blocking with 5% bovine serum albumin (BSA, 1–2 hours). Primary antibody was applied at a 1:100 dilution in 1% BSA (overnight, 4°C), samples were washed then reacted the species specific secondary antibody (Santa Cruz), and detected by VectainStain ABC Kit (Vector #PK-4000) followed by 3, 3'-diaminobenzidine (DAB) with nickel ammonium sulfate and colbalt chloride. Antibodies to osteocalcin (Takara #M173, 1:200) and Oct4A (Santa Cruz #SC5279, 1:100) were applied to paraffin sections using the same protocol as eGFP with changes to antigen retrieval: osteocalcin – trypsin only; Oct4A – 40 minutes in EDTA (pH = 9.0, 1 mM) at 98°C.

In Situ Hybridization

In situ hybridization was performed on paraffin wax embedded sections as previously described (14, 15). Subclones of mouse sox-9, type II collagen (*col2a1*), type X collagen (*col10a1*), and osteocalcin (*oc/bglp*) were linearized for transcription of DIG-labeled anti-sense riboprobes.

In Situ Cell Death Detection

Detection of apoptosis using the Roche *In Situ* Cell Death Detection Kit (Roach #116847959) according to the manufactures protocol. Sections were deparafinized, treated with proteinase-K (20 μg/mL in 10mM Tris HCl, 15 min), then reacted with the kit for 1 hour at 37 °C in the dark. Positive controls were treated with DNase I prior to the TUNEL reaction, while negative controls were not reacted with vial #1 from the kit. Slides were mounted with VectaShield with Dapi (Vector #H-1200). Apoptosis was visualized using a fluorescent microscope and photos merged with safranin-O images from adjacent slides.

Expansion of Human Mesenchymal Stem Cells

Human mesenchymal stem cells (hMSCs) were isolated and expanded from iliac crest bone marrow aspirates of consented donors as previously described (16) or purchased from Lonza (#PT-2501). hMSCs were expanded in monolayer using DMEM supplemented with 10% FBS and fibroblast growth factor 2 (FGF-2, 10 ng/ml); cells were used following 3 to 12 population doublings (passage 1–4).

hMSC Pellet Culture and In Vivo Transplantation

hMSC derived cartilage pellets were formed by putting 200,000 hMSCs into v-bottomed suspension plates, centrifuging for 5 min at 800 × *g* and culturing in a chondrogenic medium containing dexamethasone and TGF-β1 as previously described (16). Pellets were cultured for 3 weeks at 37°C with 5% CO_2 and either harvested for histology or transplanted into the tibia defect model (2–3 pellets per defect to create a tight fit).

Isolation and Culture of Human Articular Chondrocytes

Human articular chondrocytes (hACs) were obtained from the discard tissue of fresh osteochondral allografts (The Joint Restoration Foundation: male, 12–25 years, 6 donors). Chondrocytes were isolated by digesting cartilage tissue in 1% pronase (37°C, 1 hr), followed by 1–3 hours in a 0.4% collagenase type II solution (Worthington LS004176). Cells were isolated from digested tissue using a 70 μM filter, spun down to remove collagenase solution and directly encapsulated into scaffolds without expansion.

Cell Encapsulation into Poly(ethylene glycol) Diacrylate Scaffolds

Primary chondrocytes or expanded hMSC were photoencapsulated in a poly(ethylene glycol) diacrylate (PEGDA)-based semi-interpenetrating network with a scaffold composition consisting of 16% (w/v) PEGDA (6.0 kDa) and 32% (w/v) PEG-n-dimethyl ether (PEG, n=2000, MW 88kDa) to achieve a final cell density of 25×10^6 cells/ml as previously described (17, 18). Hydrogels were cultured at 37°C, 5% CO_2 for 6 weeks in defined chondrogenic medium.

mRNA isolation and quantitative RT-PCR

Murine mRNA was isolated from cartilage grafts or the entire fracture callus by homogenization in TRIzol. cDNA was reverse transcribed with Superscript III (Invitrogen #18080) and RT-PCR was performed using SYBR® Green. The primer sequences are included in Table 1. Relative gene expression was calculated by normalizing to the housekeeping gene (GAPDH, ΔC_T) and then to gene expression of the entire fracture callus, ($\Delta\Delta C_T$). Fold change was calculated as $2^{-\Delta\Delta CT}$. Graphs represent mean ± 95 % confidence of biological replicates for the cartilage grafts (n=6) or the entire fracture callus (n=5). mRNA isolation and cDNA synthesis from the hydrogels was performed as previously described (19). Relative change in gene expression was calculated by normalizing to the housekeeping gene (18S, ΔC_T) and then to gene expression of freshly isolated hACs or undifferentiated hMSCs prior to encapsulation, ($\Delta\Delta C_T$). Fold change was calculated as $2^{-\Delta\Delta CT}$. Graphs represent mean ± 95 % confidence for a total of 6 different hAC and hMSC donors.

MSC Pellet/Hydrogel Histology and Immunohistochemistry

Hydrogels were fixed in 10% neutral buffered formalin, embedded in paraffin and 5 μm sections cut onto silane coated slides. Toluidine blue staining was used to visualize sulfated proteoglycans. IHC was used to detect collagens I (1:400. Anthony Hollander), II (1:200, II-II6B3, Developmental Studies Hybridoma Bank), X (1:200. Gary Gibson) as previously described (17, 19, 20). Human mitochondria (1:100. Milipore #MAB1273) detection

followed the same protocol, but slides were treated with 0.05% trypsin (20 min at 37°C) for antigen retrieval.

In Vitro Cartilage Explant Culture Under Osteoinductive Conditions

Cartilage from the fracture callus was harvested from the central portion of the day 7 fracture as described above, rinsed with sterile PBS and then transferred into medium for *in vitro* culture at 37°C and 5% CO_2. Control medium was a serum-free high glucose DMEM containing 1% penicillin-streptomycin, 1% ITS^+ Premix (BD Biosciences Cat #354352), 1 mM sodium pyruvate, and 100 ng/ml ascorbate-2-phosphate. For osteogenic cultures, samples were grown under control conditions for two weeks, then the medium was supplemented with bone morphogenetic protein 2 (BMP-2: 10 nm, 100 nm, or 1 μm) and 10 mM β-glycerol phosphate (βGP). hMSC-derived cartilage pellets transferred to osteogenic conditions completed 3-weeks of standard chondrogenic culture prior to being transferred to osteogenic media for an additional 4 weeks of culture. Human vascular endothelial cell (HUVEC) conditioned media (HUVEC-CM) was collected from confluent plates of passage 2–3 HUVEC cells grown in Gibco Medium 200 with LVES supplement (Invitrogen #A1460901). Media was collected every 3 days; batches were combined and filter sterilized.

Histomorphometric analysis

Area of mineralization or proteoglycan deposition within the cartilage explants was determined by staining every 25th section with Alizarin Red or saffranin-O. Images were captured from a Leica DM 5000 B light microscope and number of pixels was determined by Adobe Photoshop. The volume of each was calculated using the equation for a conical frustum: $V=\frac{1}{3h}\sum_{i=1}^{n-1}(A_i+A_{i+1}+\sqrt{A_i}A_{i+1})$ Ai and Ai+1 are the area of total explant or mineralized explant extracellular matrix in sequential sections; h is the distance between sections (250 μm), and n is total number of sections analyzed per cartilage explant. Data represents the mean ± 95 % confidence of the samples and significance was tested using the Mann-Whitney U-test for non-parametric data, with p values < 0.05 determined to be significantly different. 3–6 biological replicates were used for *in vitro* quantifications.

Results

Cartilage grafts produce well-vascularized and integrated bone regenerate

The ability of a cartilage graft to stimulate bone regeneration was tested in a murine model of a segmental bone defect. External stabilization was applied to the intact tibia as previously described (12, 13), then a 2 mm osteotomy was created in mid-diaphysis and cleared of bone debris in preparation for the graft (Figure 1C). Cartilage for the graft was isolated from the central portion of a day 7 non-stabilized fracture callus by carefully dissecting the fracture callus *ex vivo* using a dissecting microscope (Figure 1A & B). The phenotype of the cartilage graft was characterized using histology, *in situ* hybridization, and quantitative RT-PCR (Figure 1). Safranin-O staining shows strong proteoglycan deposition in the graft and highlights that cellular morphology is predominantly that of normal chondrocytes with some hypertrophic chondrocytes in the middle (Figure 1D). *In situ*

hybridization confirms expression of *sox-9* and *col2a1* throughout the graft, and *col10a1* expression in hypertrophic *chondrocytes* in the central portion of the graft. *Osteocalcin (oc/bglap)* was not detected anywhere in the graft. Importantly, in regions that had low levels of safranin-O staining we observed cells expressing *sox-9* but not *oc/bglap* (Figure 1D and S2–3). Further we detected no evidence of a progenitor population using an antibody to Oct4A (Figure S8A–B). Quantitative RT-PCR analysis shows significantly more *sox-9* and *col2a1* and significantly less *oc/bglap* expression in the cartilage tissue graft compared to the entire fracture callus (Figure 1E).

A four-week healing time course of the defect shows that cartilage grafts facilitate endochondral bone repair in the mouse tibia (Figure 2). Further, the trabeculated morphology of the bone at day 28 suggest the regenerate is highly vascularized (Figure 2C). In size-matched empty defects, complete bridging of the bone was never observed (0/4), rather defects were filled largely with granulation tissue (Figure S1). Empty defects display new bone regeneration predominantly at the periosteum along with small amounts of repair tissue in the region.

Integration between the cartilage derived bone regenerate was evident histologically and tomographically (Figure 2C–D). When the healing produced from cartilage grafts was compared to living cortical bone grafts (isograft) and devitalized cortical bone grafts (allografts), cartilage was as likely to integrate with the host bone as isograft, and both were far superior to allograft (Figure 3A–B; $a = p < 0.005$). Integration strength, measured as ultimate failure by three-point bending, confirmed integration quality was not significantly different between cartilage and isograft, while integration was so poor with allograft that all grafts failed immediately without measurable force (Figure 3C). Integration strength between the host and graft at 4 weeks did not reached the full strength of uninjured cortical bone or the repair of a day 14 non-stabilized fracture that is strengthened by the excess callus tissue (Figure 3C; $b = p < 0.005$, $c = p < 0.05$). However, BMD of the isografts and cartilage grafts was not statistically different than the cortical bone controls, and, importantly the cartilage graft had a BMD equivalent to that of a day 28 fracture callus (Figure 3D; $b = p < 0.02$). BMD of the allograft was slightly higher than that of the day 14 and 21 fracture callus, and even cortical bone; increased BMD is seen in devitalized bone because it does not have the ability to remodel (Figure 3D; $b–d = p < 0.01$).

Bone regenerate is donor-derived

Based on the healing process observed above in the segmental defect, and our previous studies of endochondral fracture repair, we presumed bone regeneration from the cartilage grafts occurred through endochondral ossification in a process analogous to embryonic long bone development. This model predicts the hypertrophic chondrocytes undergo apoptosis and are replaced by osteoblasts from the host. We tested this model by transplanting cartilage from $LacZ^{+/+}$ Rosa26 mice into immunocompromised hosts and followed the fate of the regenerate using x-gal staining to detect β-galactasidase activity (specificity and endogenous/background of the x-gal staining, Figure S4). In contrast to the established model, we found that the majority of the bone regenerate was donor, rather than host, derived (Figure 3). Magnified views of the graft after four weeks of healing illustrate

transition zones where there appears to be a morphological transition of the cells from chondrocytes (Figure 3D, yellow arrow) to osteocytes (Figure 3D, yellow star) within the donor tissue. Seamless integration is observed between the graft and host tissue, with donor and host cells embedded within a continuous matrix (Figure 3C&F). Host derived chondrocytes are also evident in the tissue at the interface between the graft and host tissue (Figure 3D, green triangle), suggesting the host tissue may be stimulated either by bioactivity of the graft tissue or by mechanical stresses at the tissue interface.

The donor origin of the bone regenerate was confirmed using cartilage grafts obtained from eGFP mice and transplanted into immunocompromised mice in the same manner described above (Figure S5). Immunohistochemistry to GFP demonstrates that bone tissue was donor derived after 28 days of healing. Once again the bone regenerate appears highly trabeculated and integrates with the host tissue (Figure S5C).

Cartilage Grafts from Human MSCs also promote bone regeneration by tissue transformation

To validate the use of cartilage grafts for endochondral bone repair in a more translationally relevant system we generated cartilage pellets from human mesenchymal stem cells (hMSCs) and implanted these pellets into the murine segmental defect (Figure 4). Chondrogenesis was induced using standard pellet cultures supplemented with TGF-β1 and dexamethasone (21). Histological and immunohistochemical analysis of the hMSC-derived cartilage pellets at the time of implantation confirmed the tissue was strongly chondrogenic (Figure 4A–B) with regions of hypertrophy marked both by morphology and collagen X protein (Figure 4C). After four weeks in the tibial defects, transformation of the cartilage pellets into vascularized bone tissue was visualized with Masson's trichrome (Figure 4D–E). Donor origin of the bone was confirmed with an antibody to human mitochondria (Figure 4F). In the tibia the pellet retains it's rounded shape and integrates with the new periosteal bone formed at the cortext of the host bone.

Tissue Engineering Cartilage Grafts

Chondrogenic pellets grown by the method used in this study are inherently limited in size to approximately 1 mm in diameter, and we found that although the pellets integrated with the bone defect (Figure 4E), multiple adjacent pellets do not integrate with each other (data not shown). Consequently, scaling this methodology to larger scale (human) defects will require a different technology, such as the scaffold-based technologies developed for tissue engineering. We have previously developed a biocompatible technique for photoencapsulating hMSCs into synthetic PEGDA-based scaffolds that allow for chondrogenesis (17, 19, 20). Using this scaffold technology we tested the phenotype of cartilage that would develop from two candidate cell sources for tissue engineered cartilage: hMSCs or healthy human chondrocytes (hACs). Following 6 weeks of *in vitro* culture, sulfated proteoglycans and type II collagen were present in both hMSCs and hACs constructs, indicating their fundamental ability to generate cartilage tissue (Figure 5). However, only hMSC-encapsulated constructs elaborate collagen I and X matrix proteins, and show a robust increase in *COL10A1* and *MMP-13* gene expression.

BMP and HUVEC Conditioned medium stimulate mineralization in vitro

To better understand the role of the vasculature in converting cartilage to bone *in vivo*, cartilage tissue grafts from the fracture callus were cultured *in vitro* under osteoinductive conditions. Fracture callus cartilage cultured *in vitro* without BMP-2 maintained strong proteoglycan staining, and the cells became hypertrophic with no evidence of mineralization in the matrix (Figure 6A–C, M). When cultured with BMP-2 and β-glycerolphospate (βGP) the fracture callus cartilage mineralized, but cells maintained the hypertrophic chondrocyte morphology as opposed to becoming osteocyte-like (Figure 6D–F, M). Increasing BMP-2 concentration in culture could increase mineral content, but did not change tissue morphology (Figure S6). Similar results were obtained when MSC-derived cartilage pellets were cultured *in vitro* with BMP-2/βGP (Figure S7).

Given the incomplete morphological transformation of the explanted cartilage to bone we hypothesized biological stimuli from the vascular endothelial cells may be essential. To test this hypothesis we generated HUVEC conditioned media to simulate the fracture callus microenvironment and added it to the fracture callus cartilage cultured *in vitro*, either with or without the addition of BMP-2/βGP. HUVEC-conditioned medium alone was sufficient to produce a mineralized matrix content in the explants that was not statistically different than osteogenic medium (Figure 6G–I, M). Further addition of BMP-2/βGP to the HUVEC-conditioned medium produced a small, but not statistically significant, increase in the amount of mineralization in the cartilage explants (Figure 6J–M). Explants cultured HUVEC-conditioned also cells retained their hypertrophic morphology, perhaps due to an increase in the proteoglycan rich cartilage matrix in the explant (Figure 6M).

Endochondral fracture repair

Morphological conversion of chondrocytes into osteocytes was not completely recapitulated *in vitro* suggesting the simple replacement of soluble bioactive molecules was not sufficient to support transformation. *In vivo*, the morphological transition from chondrocyte to osteocyte is very clearly seen in the fracture callus in regions surrounding the invading vasculature (Figure 7A–D). Hypertrophic chondrocytes in these transition areas stain for both the dense collagen fibers of bone matrix (HBQ red, Figure 7A–D) and osteocalcin protein (Figure 7E–F). Adjacent to the hypertrophic chondrocytes cells appeared flatter and had the appearance of an osteocyte. To test if the switch in cell morphology was due to apoptosis of hypertrophic chondrocyte and replacement by cells from the vasculature as suggested by current models, we used an *In Situ* Cell Death Kit. At the cartilage to bone transition in day 7 (Figure 7G) and day 10 (Figure 7H) fracture calluses the majority of the apoptosis occurred in cells that histologically and morphologically identified as bone cells, as opposed to hypertrophic chondrocytes. This data suggests that apoptosis may simply facilitate remodeling of the hard callus to create marrow space. We next looked to see if progenitor programs were being activated in the hypertrophic chondrocytes transition areas that could enable a phenotypic reprogramming of these cells. Oct4A appears to be present in hypertrophic chondrocytes in transition areas near the vasculature (Figure 7I–J and S8C–D). We did not see evidence of Oct4A in chondrocytes or hypotrophic chondrocytes in areas without invading vasculature (Figure S8E–E), or in the newly formed bone following the transition (Figure S8G–H).

Discussion

The ability to regenerate a vascularized bone using tissue grafts is presently constrained by the clinical limitations of current technologies. While autograft bone procedures produce reasonably successful outcomes, donor site morbidity and quantity of available tissue are significant problems (22, 23). Clinical failures associated with allografts have been extensively documented in both animal and human studies. The main problem is that the tissue remains inert, producing limited revitalization and eventual loss in structural integrity of the graft (5, 10, 24–26). A major effort has been made to develop novel technologies to promote vascularization during bone regeneration using gene therapy or growth factor delivery of VEGF (11, 27–30). In this study we investigated an alternative approach for stimulating vascularized bone regeneration using cartilage tissue grafts to promote endochondral bone repair. Using a translational murine model of segmental bone defects we demonstrated that transplanted cartilage produces a highly trabeculated and well vascularized bone regenerate that integrates well with the host tissue.

The specific advantage that cartilage grafts offer over bone transplantation is likely associated with the inherent bioactivity of chondrocytes and their adaptation for function under avascular conditions. As chondrocytes mature towards hypertrophy they secrete VEGF to stimulate vascular invasion, MMP-13 to promote mineralization of the extracellular matrix, and BMPs to promote osteogenesis (31–34). Capitalizing on this innate biological function may eliminate the need for complex engineering strategies to deliver bioactive stimuli. Further, chondrocytes are metabolically optimized for avascular conditions (35) providing a therapeutic advantage for bone repair since grafting is often required in areas of vascular damage. Ischemia is detrimental to osteogenesis and significantly increases the rate of fracture non-union (36, 37) and contributes to current bone graft failures (4).

The concept of using cartilage to promote endochondral bone regeneration has been effectively overlooked at a clinical level despite the clear biological relevance of this approach. In this study we generated endochondral cartilage by creating unstabilized fractures in murine tibiae and by inducing hMSCs towards chondrogenesis. Previous experiments have demonstrated the capacity of cartilage with a hypertrophic phenotype to form bone both *in vitro* (38–41) and after ectopic transplantation (41–45). Interestingly, hyaline cartilage, which does not express collagens I or X, appears to be privileged from this transition to bone and similar experiments have been unable to induce these “permanent” chondrocytes to undergo endochondral ossification ((41, 43, 45, 46), and data not shown). Consequently, endochondral cartilage, or specifically the ability to undergo hypertrophic maturation, appears requisite in supporting bone regeneration. Functional bone organ regeneration by endochondral ossification has demonstrated that complete bone tissue can be produced from hMSC-derived cartilage (47, 48); validating the concept explored here that recapitulating developmental sequences may be a useful tissue engineering strategy. Our data expand upon these studies to show that endochondral cartilage can promote effective healing of a segmental bone defect in a clinically relevant model. Specifically the bone regenerate produced by the cartilage graft is highly vascularized and integrates much better than allograft bone, and the cartilage graft integrated as well as isograft. The isograft

and allograft models used for this study have been previously described in a murine long bone defect study (9–11), provided for consistent graft dimensions for comparison across grafting groups, and have clinical relevance for the treatment of human bone defects with large segment grafting.

A key feature of our study is that we utilized genetic labels on the cartilage grafts to track the contribution of the donor versus host to the bone regenerate. Our hypothesis was that the cartilage graft would create a template for bone remodeling in a similar fashion to endochondral ossification during development: by this model the transplanted chondrocytes would undergo apoptosis and the bone would be host derived. In contrast to our hypothesis, the bone regenerate was largely donor derived. This was verified using two different genetically labeled mouse strains, Rosa26 (Lac-Z-positive) and eGFP, and a human mitochondria stain to identify origin of the transplanted hMSC-derived cartilage pellets. In line with our transplant results, both Scotti *et al* (44) and Sacchetti *et al* (49) have found that the ectopic bone formed from subcutaneously transplanted hMSC-cartilage was donor derived. However, because of the potential heterogeneity in the cartilage tissue grafts, neither our study, nor the previous works, can conclusively refute the argument that the graft already contains committed osteocytes, or that a small population of donor derived osteoprogenitor cells could re-populate the bone regenerate. To address the possibility that osteoblasts were present in the cartilage graft we used qRT-PCR and *in situ* hybridization to confirm *sox-9* expression throughout the graft and demonstrated that there was no molecular evidence of osteoblasts. Further, we saw no expression of the stem cell marker Oct4A in the cartilage graft prior to transplantation suggesting progenitor cells were not present. Oct4A is an established marker of pluripotent stem cells, although its role in adult stem cell populations is not clear. Presently there are no good markers for mouse MSCs and the absence of Oct4A cannot conclusively demonstrate osteoprogenitors were not present.

The donor-fate of the bone regenerate prompted us to examine the fracture callus to evaluate whether endochondral repair may differ from the traditional view of endochondral ossification during development. In regions containing the cartilage to bone transition in the fracture callus (“transition zone”), there is an obvious phenotypic maturation of chondrocyte to hypertrophic chondrocyte to bone near the vasculature. We found limited evidence of apoptosis in hypertrophic chondrocytes at these transition zones. This result is supported by other studies showing that the hypertrophic chondrocytes may not be destined for apoptosis (50–54). This does not exclude the possibility that cells from the invading vasculature also contribute to bone formation (55), but rather suggests that invading cells may not be the only (56), or even primary, method by which bone is formed during endochondral repair.

This study is not the first to suggest that cartilage can become bone, but the idea remains non-dogmatic and it is presently not clear whether this happens routinely during development and repair, or only under certain circumstances. Further, if cartilage to bone transformation does occur, it is unclear which genetic or molecular sequences enable this change. While some reports suggest that cartilage “dedifferentiates” to a progenitor-like state before becoming bone (51, 57), other data supports a mechanism where chondrocytes can mature directly into osteocytes (50, 56, 58–63). In our study we found that hypertrophic chondrocytes at the transition zone of the fracture callus appear to express the progenitor

marker Oct4A. The mechanism by which Oct4A acts is not completely understood: in this situation the chondrocytes could be dedifferentiating to regain progenitor capabilities, similar to induced pluripotent cells, and consistent with the mechanism described by Song & Tuan (57). Alternatively Oct4A may function differently in adult somatic cells and allow cellular reprogramming to enable a direct transition from cartilage to bone. Further work is required to elucidate the extent to which Oct4A may reprogram the chondrocytes during fracture healing. A significant challenge towards learning the mechanistic details of transformation is the substantial overlap between markers of hypertrophic chondrocytes and osteoblasts (64–67). Consequently, lineage tracing and clearly defining cartilage versus bone tissue is difficult both *in vitro* and *in vivo* and relies heavily of differences in morphology.

Based on this data we hypothesized the vasculature is essential in coordinating the phenotypic transformation from cartilage to bone. To isolate the vasculature from the experiment we cultured the cartilage grafts *in vitro* under osteogenic conditions containing BMP-2. The fracture callus cartilage explants largely maintained their hypertrophic morphology and regions of calcification and cartilage matrix staining overlapped. For the hMSC pellets, regions of mineralization generally occurred in areas where there was diminished proteogylcan content and more flattened cells were observed. The ability of MSC-derived cartilage to generate these so-called “chondro-osseo rudiments” *in vitro* has previously been described, demonstrating that this superficial region has the histological, ultrastructural, and immunohistochemical characteristics of bone (38).

To more accurately recapitulate the microenvironment of the fracture callus *in vitro*, and specifically introduce the paracrine effect of vascular endothelial cells, we cultured the cartilage explants with HUVEC conditioned medium. The invading vascular endothelial cells provide MMP-9 (68) and BMPs (33, 69) to stimulate alkaline phosphatase activity (70), but the complete set of bioactive stimuli is not fully defined. We found that this media was sufficient to promote mineralization of the cartilage matrix, but still did not observe substantial morphological change of the hypertrophic chondrocyte to osteocyte. Taken together these *in vitro* experiments suggest that while mineralized cartilage can be produced with soluble factors from vascular endothelial cells, or BMP-2 treatment, they alone are not sufficient to produce a complete transition to bone.

Degradation of the cartilage matrix and mechanical stimulation were two components of the *in vivo* environment that were not replicated by our *in vitro* conditions. Previous data from our laboratory has shown that cartilage remodeling is critical during fracture repair and the absence of MMPs results in impaired healing (32, 68). Similarly, our laboratory has shown that mechanical stability influences the fate of skeletal progenitor cells during bone healing, with full stabilization promoting intramembranous repair and movement enabling endochondral ossification (13). The role of mechanical loading during the transition cartilage to bone in the fracture callus has not been previously explored. It is possible that mechanical stimulation is central to this transition and contributed to the sustained hypertrophic phenotype observed *in vitro* and enabled the transition in the segmental defect. The murine model used in this study, while providing external stabilization to facilitate alignment, will not completely eliminate sheer and compressive forces between the host and graft bone. The precise effect of loading in regulating the transformation of cartilage to

bone, both at a molecular or kinetic level, were not explored in this study, but are important questions to consider in larger animal models.

Designing improved clinical treatments for repair and regeneration of bone is a central focus of our laboratory. Our study substantiates the concept of using cartilage grafts as an alternative therapeutic approach for bone regeneration. Further, evidence that the cartilage directly converts into bone during repair may also require change in how we approach the treatment of impaired healing in fractures. Full realization of the cartilage graft technology described in this study is presently limited by the ability to scale this approach to clinically relevant defects; a next step for this study will be to optimize a scaffold for a tissue engineering strategy (19) and translate this approach into a large animal study. The importance of understanding the mechanism by which cartilage can regenerate bone for therapeutic purposes comes in designing an appropriate tissue engineering approach to accurately recapitulate the regeneration sequences.

Supplementary Material

Refer to Web version on PubMed Central for supplementary material.

Acknowledgments

Some materials and reagents were generously gifted from colleagues: Jennifer West (Rice University, 6kDa PEGDA), Gary Gibson (Henry Ford, Collagen X antibody), Anthony Hollender, (University of Bristol, Collagen I antibody), Francesco Curcio (Oct4A antibody). We would also like to thank colleagues Alfred Kuo, Tamara Alliston, Nathan Young, and Brian Hall for their thoughtful review and discussion of our data. Thank you to Frank Yang for his assistance with murine husbandry and fractures, Alexis Lainoff for preparation of some of the probes for *in situ*, and to Gina Baldoza and Anna Lissa Wi for daily lab function and grants administration.

Grant Support

Research reported in this publication was supported by the National Institute of Arthritis and Musculoskeletal and Skin Disease (NIAMS) of the National Institutes of Health (NIH) under the following award numbers: CSB (#5F32AR062469-02), TM (#AR053645), and TM (#AR057344). Additional research support was provided by the Musculoskeletal Transplant Foundation (CSB: MTF Junior Investigator Award), the UCSF Graduate Education in Medical Sciences (GEMS) & Clinical and Translational Science Institute (CTSI), OHSU Gerlinger Research Award (BJ, CSB).

REFERENCES

1. Lim SS, Vos T, Flaxman AD, Danaei G, Shibuya K, Adair-Rohani H, et al. A comparative risk assessment of burden of disease and injury attributable to 67 risk factors and risk factor clusters in 21 regions, 1990–2010: a systematic analysis for the Global Burden of Disease Study 2010. Lancet. 2012; 380(9859):2224–2260. Epub 2012/12/19. doi: 10.1016/S0140-6736(12)61766-8 S0140-6736(12)61766-8 [pii]. PubMed PMID: 23245609. [PubMed: 23245609]
2. Agency for Healthcare Research and Quality. Available from: http://www.ahrq.gov/news/nn/nn012506.htm
3. The Burden of Musculoskeletal Diseases in the United States. Rosemont, IL: American Academy of Orthopaedic Surgeons; 2008.
4. Nguyen LH, Annabi N, Nikkhah M, Bae H, Binan L, Park S, et al. Vascularized bone tissue engineering: approaches for potential improvement. Tissue engineering Part B, Reviews. 2012; 18(5):363–382. PubMed PMID: 22765012; PubMed Central PMCID: PMC3458624. [PubMed: 22765012]

5. Brigman BE, Hornicek FJ, Gebhardt MC, Mankin HJ. Allografts about the Knee in Young Patients with High-Grade Sarcoma. Clinical orthopaedics and related research. 2004; (421):232–239. Epub 2004/05/05. PubMed PMID: 15123953. [PubMed: 15123953]

6. Kronenberg HM. Developmental regulation of the growth plate. Nature. 2003; 423(6937):332–336. Epub 2003/05/16. doi: 10.1038/nature01657 nature01657 [pii]. PubMed PMID: 12748651. [PubMed: 12748651]

7. Colnot C, Lu C, Hu D, Helms JA. Distinguishing the contributions of the perichondrium, cartilage, and vascular endothelium to skeletal development. Dev Biol. 2004; 269(1):55–69. Epub 2004/04/15. doi: 10.1016/j.ydbio.2004.01.011 S0012160604000454 [pii]. PubMed PMID: 15081357. [PubMed: 15081357]

8. Little DG, Ramachandran M, Schindeler A. The anabolic and catabolic responses in bone repair. The Journal of bone and joint surgery British volume. 2007; 89(4):425–433. Epub 2007/04/28. doi: 10.1302/0301-620X.89B4.18301. PubMed PMID: 17463107. [PubMed: 17463107]

9. Tiyapatanaputi P, Rubery PT, Carmouche J, Schwarz EM, O'Keefe RJ, Zhang X. A novel murine segmental femoral graft model. Journal of orthopaedic research : official publication of the Orthopaedic Research Society. 2004; 22(6):1254–1260. Epub 2004/10/12. doi: 10.1016/j.orthres.2004.03.017. PubMed PMID: 15475206. [PubMed: 15475206]

10. Lee FY, Hazan EJ, Gebhardt MC, Mankin HJ. Experimental model for allograft incorporation and allograft fracture repair. Journal of orthopaedic research : official publication of the Orthopaedic Research Society. 2000; 18(2):303–306. Epub 2000/05/18. doi: 10.1002/jor.1100180219. PubMed PMID: 10815832. [PubMed: 10815832]

11. Ito H, Koefoed M, Tiyapatanaputi P, Gromov K, Goater JJ, Carmouche J, et al. Remodeling of cortical bone allografts mediated by adherent rAAV-RANKL and VEGF gene therapy. Nature medicine. 2005; 11(3):291–297. Epub 2005/02/16. doi: nm1190 [pii] 10.1038/nm1190. PubMed PMID: 15711561; PubMed Central PMCID: PMC1364464.

12. Yu YY, Bahney C, Hu D, Marcucio RS, Miclau T 3rd. Creating rigidly stabilized fractures for assessing intramembranous ossification, distraction osteogenesis, or healing of critical sized defects. J Vis Exp. 2012; (62) Epub 2012/04/25. doi: 10.3791/3552 3552 [pii]. PubMed PMID: 22525683.

13. Thompson Z, Miclau T, Hu D, Helms JA. A model for intramembranous ossification during fracture healing. Journal of orthopaedic research : official publication of the Orthopaedic Research Society. 2002; 20(5):1091–1098. Epub 2002/10/18. doi: 10.1016/S0736-0266(02)00017-7. PubMed PMID: 12382977. [PubMed: 12382977]

14. Hu D, Marcucio RS. A SHH-responsive signaling center in the forebrain regulates craniofacial morphogenesis via the facial ectoderm. Development. 2009; 136(1):107–116. Epub 2008/11/28. doi: 10.1242/dev.026583. PubMed PMID: 19036802; PubMed Central PMCID: PMC2685963. [PubMed: 19036802]

15. Rumballe B, Georgas K, Little MH. High-throughput paraffin section in situ hybridization and dual immunohistochemistry on mouse tissues. CSH protocols. 2008; 2008 pdb prot5030. Epub 2008/01/01. doi: 10.1101/pdb.prot5030. PubMed PMID: 21356874; PubMed Central PMCID: PMC2725362.

16. Johnstone B, Hering TM, Caplan AI, Goldberg VM, Yoo JU. In vitro chondrogenesis of bone marrow-derived mesenchymal progenitor cells. Exp Cell Res. 1998; 238(1):265–272. Epub 1998/02/11. doi: S0014-4827(97)93858-1 [pii] 10.1006/excr.1997.3858. PubMed PMID: 9457080. [PubMed: 9457080]

17. Buxton AN, Bahney CS, Yoo J, Johnstone B. Temporal Exposure to Chondrogenic Factors Modulates Human Mesenchymal Stem Cell Chondrogenesis in Hydrogels. Tissue Eng Part A. 2010 Epub 2010/08/31. doi: 10.1089/ten.TEA.2009.0839. PubMed PMID: 20799905.

18. Buxton AN, Zhu J, Marchant R, West JL, Yoo JU, Johnstone B. Design and characterization of poly(ethylene glycol) photopolymerizable semi-interpenetrating networks for chondrogenesis of human mesenchymal stem cells. Tissue engineering. 2007; 13(10):2549–2560. Epub 2007/07/28. doi: 10.1089/ten.2007.0075. PubMed PMID: 17655489. [PubMed: 17655489]

19. Bahney CS, Hsu CW, Yoo JU, West JL, Johnstone B. A bioresponsive hydrogel tuned to chondrogenesis of human mesenchymal stem cells. FASEB J. 2011; 25(5):1486–1496. Epub

2011/02/02. doi: fj. 10-165514 [pii] 10.1096/fj.10-165514. PubMed PMID: 21282205. [PubMed: 21282205]

20. Bahney CS, Hsu CW, Bottlang M, West JL, Johnstone B. Visible light photoinitiation of mesenchymal stem cell-laden bioresponsive hydrogels. Eur Cell Mater. 2011; 22:43–55. Epub 2011/07/16. doi: vol022a04 [pii]. PubMed PMID: 21761391. [PubMed: 21761391]
21. Yoo JU, Barthel TS, Nishimura K, Solchaga L, Caplan AI, Goldberg VM, et al. The chondrogenic potential of human bone-marrow-derived mesenchymal progenitor cells. The Journal of bone and joint surgery American volume. 1998; 80(12):1745–1757. Epub 1999/01/06. PubMed PMID: 9875932. [PubMed: 9875932]
22. Burchardt H, Enneking WF. Transplantation of bone. The Surgical clinics of North America. 1978; 58(2):403–427. Epub 1978/04/01. PubMed PMID: 349741. [PubMed: 349741]
23. De Long WG Jr, Einhorn TA, Koval K, McKee M, Smith W, Sanders R, et al. Bone grafts and bone graft substitutes in orthopaedic trauma surgery. A critical analysis. The Journal of bone and joint surgery American volume. 2007; 89(3):649–658. PubMed PMID: 17332116. [PubMed: 17332116]
24. Benevenia J, Zimmerman M, Keating J, Cyran F, Blacksin M, Parsons JR. Mechanical environment affects allograft incorporation. Journal of biomedical materials research. 2000; 53(1): 67–72. Epub 2000/01/15. PubMed PMID: 10634954. [PubMed: 10634954]
25. Enneking WF, Campanacci DA. Retrieved human allografts : a clinicopathological study. The Journal of bone and joint surgery American volume. 2001; 83-A(7):971–986. Epub 2001/07/14. PubMed PMID: 11451965. [PubMed: 11451965]
26. Wheeler DL, Enneking WF. Allograft bone decreases in strength in vivo over time. Clinical orthopaedics and related research. 2005; (435):36–42. Epub 2005/06/03. PubMed PMID: 15930919. [PubMed: 15930919]
27. Hiltunen MO, Ruuskanen M, Huuskonen J, Mahonen AJ, Ahonen M, Rutanen J, et al. Adenovirus-mediated VEGF-A gene transfer induces bone formation in vivo. FASEB J. 2003; 17(9):1147–1149. Epub 2003/04/15. doi: 10.1096/fj.02-0514fje. PubMed PMID: 12692089. [PubMed: 12692089]
28. Kaigler D, Wang Z, Horger K, Mooney DJ, Krebsbach PH. VEGF scaffolds enhance angiogenesis and bone regeneration in irradiated osseous defects. J Bone Miner Res. 2006; 21(5):735–744. Epub 2006/06/01. doi: 10.1359/jbmr.060120. PubMed PMID: 16734388. [PubMed: 16734388]
29. Leach JK, Kaigler D, Wang Z, Krebsbach PH, Mooney DJ. Coating of VEGF-releasing scaffolds with bioactive glass for angiogenesis and bone regeneration. Biomaterials. 2006; 27(17):3249–3255. Epub 2006/02/24. doi: 10.1016/j.biomaterials.2006.01.033. PubMed PMID: 16490250. [PubMed: 16490250]
30. Zisch AH, Lutolf MP, Ehrbar M, Raeber GP, Rizzi SC, Davies N, et al. Cell-demanded release of VEGF from synthetic, biointeractive cell ingrowth matrices for vascularized tissue growth. FASEB J. 2003; 17(15):2260–2262. Epub 2003/10/18. doi: 10.1096/fj.02-1041fje 02-1041fje [pii]. PubMed PMID: 14563693. [PubMed: 14563693]
31. Gerber HP, Vu TH, Ryan AM, Kowalski J, Werb Z, Ferrara N. VEGF couples hypertrophic cartilage remodeling, ossification and angiogenesis during endochondral bone formation. Nature medicine. 1999; 5(6):623–628. Epub 1999/06/17. doi: 10.1038/9467. PubMed PMID: 10371499.
32. Behonick DJ, Xing Z, Lieu S, Buckley JM, Lotz JC, Marcucio RS, et al. Role of matrix metalloproteinase 13 in both endochondral and intramembranous ossification during skeletal regeneration. PloS one. 2007; 2(11):e1150. Epub 2007/11/08. doi: 10.1371/journal.pone.0001150. PubMed PMID: 17987127; PubMed Central PMCID: PMC2063465. [PubMed: 17987127]
33. Yu YY, Lieu S, Lu C, Miclau T, Marcucio RS, Colnot C. Immunolocalization of BMPs, BMP antagonists, receptors, and effectors during fracture repair. Bone. 2010; 46(3):841–851. Epub 2009/11/17. doi: S8756-3282(09)02017-1 [pii] 10.1016/j.bone.2009.11.005. PubMed PMID: 19913648. [PubMed: 19913648]
34. Gerstenfeld LC, Cruceta J, Shea CM, Sampath K, Barnes GL, Einhorn TA. Chondrocytes provide morphogenic signals that selectively induce osteogenic differentiation of mesenchymal stem cells. J Bone Miner Res. 2002; 17(2):221–230. Epub 2002/01/29. doi: 10.1359/jbmr.2002.17.2.221. PubMed PMID: 11811552. [PubMed: 11811552]

35. Schipani E. Hypoxia and HIF-1alpha in chondrogenesis. Annals of the New York Academy of Sciences. 2006; 1068:66–73. PubMed PMID: 16831906. [PubMed: 16831906]

36. Lu C, Miclau T, Hu D, Marcucio RS. Ischemia leads to delayed union during fracture healing: a mouse model. Journal of orthopaedic research : official publication of the Orthopaedic Research Society. 2007; 25(1):51–61. Epub 2006/10/05. doi: 10.1002/jor.20264. PubMed PMID: 17019699; PubMed Central PMCID: PMC2848995. [PubMed: 17019699]

37. Dickson KF, Katzman S, Paiement G. The importance of the blood supply in the healing of tibial fractures. Contemp Orthop. 1995; 30(6):489–493. Epub 1995/05/08. PubMed PMID: 10150380. [PubMed: 10150380]

38. Muraglia A, Cancedda R, Quarto R. Clonal mesenchymal progenitors from human bone marrow differentiate in vitro according to a hierarchical model. J Cell Sci. 2000; 113(Pt 7):1161–1166. Epub 2000/03/08. PubMed PMID: 10704367. [PubMed: 10704367]

39. Oliveira SM, Amaral IF, Barbosa MA, Teixeira CC. Engineering endochondral bone: in vitro studies. Tissue Eng Part A. 2009; 15(3):625–634. Epub 2008/09/02. doi: 10.1089/ten.tea.2008.0051. PubMed PMID: 18759672; PubMed Central PMCID: PMC2744199. [PubMed: 18759672]

40. Riminucci M, Bradbeer JN, Corsi A, Gentili C, Descalzi F, Cancedda R, et al. Vis-a-vis cells and the priming of bone formation. J Bone Miner Res. 1998; 13(12):1852–1861. Epub 1998/12/09. doi: 10.1359/jbmr.1998.13.12.1852. PubMed PMID: 9844103. [PubMed: 9844103]

41. Jukes JM, Both SK, Leusink A, Sterk LM, van Blitterswijk CA, de Boer J. Endochondral bone tissue engineering using embryonic stem cells. Proc Natl Acad Sci U S A. 2008; 105(19):6840–6845. Epub 2008/05/10. doi: 10.1073/pnas.0711662105. PubMed PMID: 18467492; PubMed Central PMCID: PMC2374550. [PubMed: 18467492]

42. Dickhut A, Pelttari K, Janicki P, Wagner W, Eckstein V, Egermann M, et al. Calcification or dedifferentiation: requirement to lock mesenchymal stem cells in a desired differentiation stage. J Cell Physiol. 2009; 219(1):219–226. Epub 2008/12/25. doi: 10.1002/jcp.21673. PubMed PMID: 19107842. [PubMed: 19107842]

43. Pelttari K, Winter A, Steck E, Goetzke K, Hennig T, Ochs BG, et al. Premature induction of hypertrophy during in vitro chondrogenesis of human mesenchymal stem cells correlates with calcification and vascular invasion after ectopic transplantation in SCID mice. Arthritis Rheum. 2006; 54(10):3254–3266. Epub 2006/09/30. doi: 10.1002/art.22136. PubMed PMID: 17009260. [PubMed: 17009260]

44. Scotti C, Tonnarelli B, Papadimitropoulos A, Scherberich A, Schaeren S, Schauerte A, et al. Recapitulation of endochondral bone formation using human adult mesenchymal stem cells as a paradigm for developmental engineering. Proc Natl Acad Sci U S A. 2010; 107(16):7251–7256. Epub 2010/04/22. doi: 10.1073/pnas.1000302107. PubMed PMID: 20406908; PubMed Central PMCID: PMC2867676. [PubMed: 20406908]

45. Oliveira SM, Mijares DQ, Turner G, Amaral IF, Barbosa MA, Teixeira CC. Engineering endochondral bone: in vivo studies. Tissue Eng Part A. 2009; 15(3):635–643. Epub 2008/09/02. doi: 10.1089/ten.tea.2008.0052. PubMed PMID: 18759673; PubMed Central PMCID: PMC2751848. [PubMed: 18759673]

46. Vacanti CA, Kim W, Upton J, Mooney D, Vacanti JP. The efficacy of periosteal cells compared to chondrocytes in the tissue engineered repair of bone defects. Tissue engineering. 1995; 1(3):301–308. Epub 1995/10/01. doi: 10.1089/ten.1995.1.301. PubMed PMID: 19877908. [PubMed: 19877908]

47. Scotti C, Piccinini E, Takizawa H, Todorov A, Bourgine P, Papadimitropoulos A, et al. Engineering of a functional bone organ through endochondral ossification. Proc Natl Acad Sci U S A. 2013; 110(10):3997–4002. Epub 2013/02/13. doi: 10.1073/pnas.1220108110. PubMed PMID: 23401508; PubMed Central PMCID: PMC3593845. [PubMed: 23401508]

48. Huang JI, Durbhakula MM, Angele P, Johnstone B, Yoo JU. Lunate arthroplasty with autologous mesenchymal stem cells in a rabbit model. The Journal of bone and joint surgery American volume. 2006; 88(4):744–752. Epub 2006/04/06. doi: 88/4/744 [pii] 10.2106/JBJS.E.00669. PubMed PMID: 16595464. [PubMed: 16595464]

49. Sacchetti B, Funari A, Michienzi S, Di Cesare S, Piersanti S, Saggio I, et al. Self-renewing osteoprogenitors in bone marrow sinusoids can organize a hematopoietic microenvironment. Cell.

2007; 131(2):324–336. Epub 2007/10/25. doi: S0092-8674(07)01087-2 [pii] 10.1016/j.cell.2007.08.025. PubMed PMID: 17956733. [PubMed: 17956733]

50. Roach HI. New aspects of endochondral ossification in the chick: chondrocyte apoptosis, bone formation by former chondrocytes, and acid phosphatase activity in the endochondral bone matrix. J Bone Miner Res. 1997; 12(5):795–805. Epub 1997/05/01. doi: 10.1359/jbmr.1997.12.5.795. PubMed PMID: 9144346. [PubMed: 9144346]
51. Hall, BK. Bones and Cartilage: Developmental and Evolutionary Skeletal Biology. 1. Academic Press; 2005. Dedifferntiation Provides Progenitor Cells for Jaws and Long Bones; p. 166-82.
52. Yoshioka C, Yagi T. Electron microscopic observations on the fate of hypertrophic chondrocytes in condylar cartilage of rat mandible. Journal of craniofacial genetics and developmental biology. 1988; 8(3):253–264. PubMed PMID: 3209687. [PubMed: 3209687]
53. Kuhlman RE, McNamee MJ. The biochemical importance of the hypertrophic cartilage cell area to enchondral bone formation. The Journal of bone and joint surgery American volume. 1970; 52(5): 1025–1032. PubMed PMID: 5479473. [PubMed: 5479473]
54. Holtrop ME. The ultrastructure of the epiphyseal plate. II. The hypertrophic chondrocyte. Calcified tissue research. 1972; 9(2):140–151. PubMed PMID: 4339942. [PubMed: 4339942]
55. Maes C, Kobayashi T, Selig MK, Torrekens S, Roth SI, Mackem S, et al. Osteoblast precursors, but not mature osteoblasts, move into developing and fractured bones along with invading blood vessels. Dev Cell. 2010; 19(2):329–344. Epub 2010/08/17. doi: S1534-5807(10)00338-2 [pii] 10.1016/j.devcel.2010.07.010. PubMed PMID: 20708594. [PubMed: 20708594]
56. Yasui N, Sato M, Ochi T, Kimura T, Kawahata H, Kitamura Y, et al. Three modes of ossification during distraction osteogenesis in the rat. The Journal of bone and joint surgery British volume. 1997; 79(5):824–830. Epub 1997/10/23. PubMed PMID: 9331045. [PubMed: 9331045]
57. Song L, Tuan RS. Transdifferentiation potential of human mesenchymal stem cells derived from bone marrow. FASEB J. 2004; 18(9):980–982. Epub 2004/04/16. doi: 10.1096/fj.03-1100fje 03-1100fje [pii]. PubMed PMID: 15084518. [PubMed: 15084518]
58. Roach HI. Trans-differentiation of hypertrophic chondrocytes into cells capable of producing a mineralized bone matrix. Bone Miner. 1992; 19(1):1–20. Epub 1992/10/01. PubMed PMID: 1422302. [PubMed: 1422302]
59. Scammell BE, Roach HI. A new role for the chondrocyte in fracture repair: endochondral ossification includes direct bone formation by former chondrocytes. J Bone Miner Res. 1996; 11(6):737–745. Epub 1996/06/01. doi: 10.1002/jbmr.5650110604. PubMed PMID: 8725170. [PubMed: 8725170]
60. Galotto M, Campanile G, Robino G, Cancedda FD, Bianco P, Cancedda R. Hypertrophic chondrocytes undergo further differentiation to osteoblast-like cells and participate in the initial bone formation in developing chick embryo. J Bone Miner Res. 1994; 9(8):1239–1249. Epub 1994/08/01. doi: 10.1002/jbmr.5650090814. PubMed PMID: 7976506. [PubMed: 7976506]
61. Pritchard JJ, Ruzicka AJ. Comparison of fracture repair in the frog, lizard and rat. Journal of anatomy. 1950; 84(3):236–261. PubMed PMID: 15436329; PubMed Central PMCID: PMC1273300. [PubMed: 15436329]
62. Kawakami T, Kawai T, Kimura A, Hasegawa H, Tsujigiwa H, Gunduz M, et al. Characteristics of Bone Morphogenetic Protein-induced Chondroid Bone: Histochemical, Immunohistochemical and in situ Hybridization Examinations. The Journal of International Medical Research. 2001; 29(6)
63. Aigner T, Loos S, Muller S, Sandell LJ, Unni KK, Kirchner T. Cell differentiation and matrix gene expression in mesenchymal chondrosarcomas. The American journal of pathology. 2000; 156(4): 1327–1335. Epub 2000/04/07. doi: 10.1016/S0002-9440(10)65003-1. PubMed PMID: 10751358; PubMed Central PMCID: PMC1876868. [PubMed: 10751358]
64. Hughes SS, Hicks DG, O'Keefe RJ, Hurwitz SR, Crabb ID, Krasinskas AM, et al. Shared phenotypic expression of osteoblasts and chondrocytes in fracture callus. J Bone Miner Res. 1995; 10(4):533–544. PubMed PMID: 7610923. [PubMed: 7610923]
65. Gerstenfeld LC, Shapiro FD. Expression of bone-specific genes by hypertrophic chondrocytes: implication of the complex functions of the hypertrophic chondrocyte during endochondral bone development. Journal of cellular biochemistry. 1996; 62(1):1–9. Epub 1996/07/01. doi: 10.1002/

(SICI)1097-4644(199607)62:1<1::AID-JCB1>3.0.CO;2-X. PubMed PMID: 8836870. [PubMed: 8836870]

66. Lian JB, McKee MD, Todd AM, Gerstenfeld LC. Induction of bone-related proteins, osteocalcin and osteopontin, and their matrix ultrastructural localization with development of chondrocyte hypertrophy in vitro. Journal of cellular biochemistry. 1993; 52(2):206–219. Epub 1993/06/01. doi: 10.1002/jcb.240520212. PubMed PMID: 8366137. [PubMed: 8366137]
67. Stafford HJ, Roberts MT, Oni OO, Hay J, Gregg P. Localisation of bone-forming cells during fracture healing by osteocalcin immunocytochemistry: an experimental study of the rabbit tibia. Journal of orthopaedic research : official publication of the Orthopaedic Research Society. 1994; 12(1):29–39. PubMed PMID: 8113940. [PubMed: 8113940]
68. Colnot C, Thompson Z, Miclau T, Werb Z, Helms JA. Altered fracture repair in the absence of MMP9. Development. 2003; 130(17):4123–4133. Epub 2003/07/23. PubMed PMID: 12874132; PubMed Central PMCID: PMC2778064. [PubMed: 12874132]
69. Matsubara H, Hogan DE, Morgan EF, Mortlock DP, Einhorn TA, Gerstenfeld LC. Vascular tissues are a primary source of BMP2 expression during bone formation induced by distraction osteogenesis. Bone. 2012; 51(1):168–180. PubMed PMID: 22391215. [PubMed: 22391215]
70. Kang Y, Kim S, Fahrenholtz M, Khademhosseini A, Yang Y. Osteogenic and angiogenic potentials of monocultured and co-cultured human-bone-marrow-derived mesenchymal stem cells and human-umbilical-vein endothelial cells on three-dimensional porous beta-tricalcium phosphate scaffold. Acta biomaterialia. 2013; 9(1):4906–4915. Epub 2012/08/21. doi: 10.1016/j.actbio.2012.08.008. PubMed PMID: 22902820; PubMed Central PMCID: PMC3508299. [PubMed: 22902820]

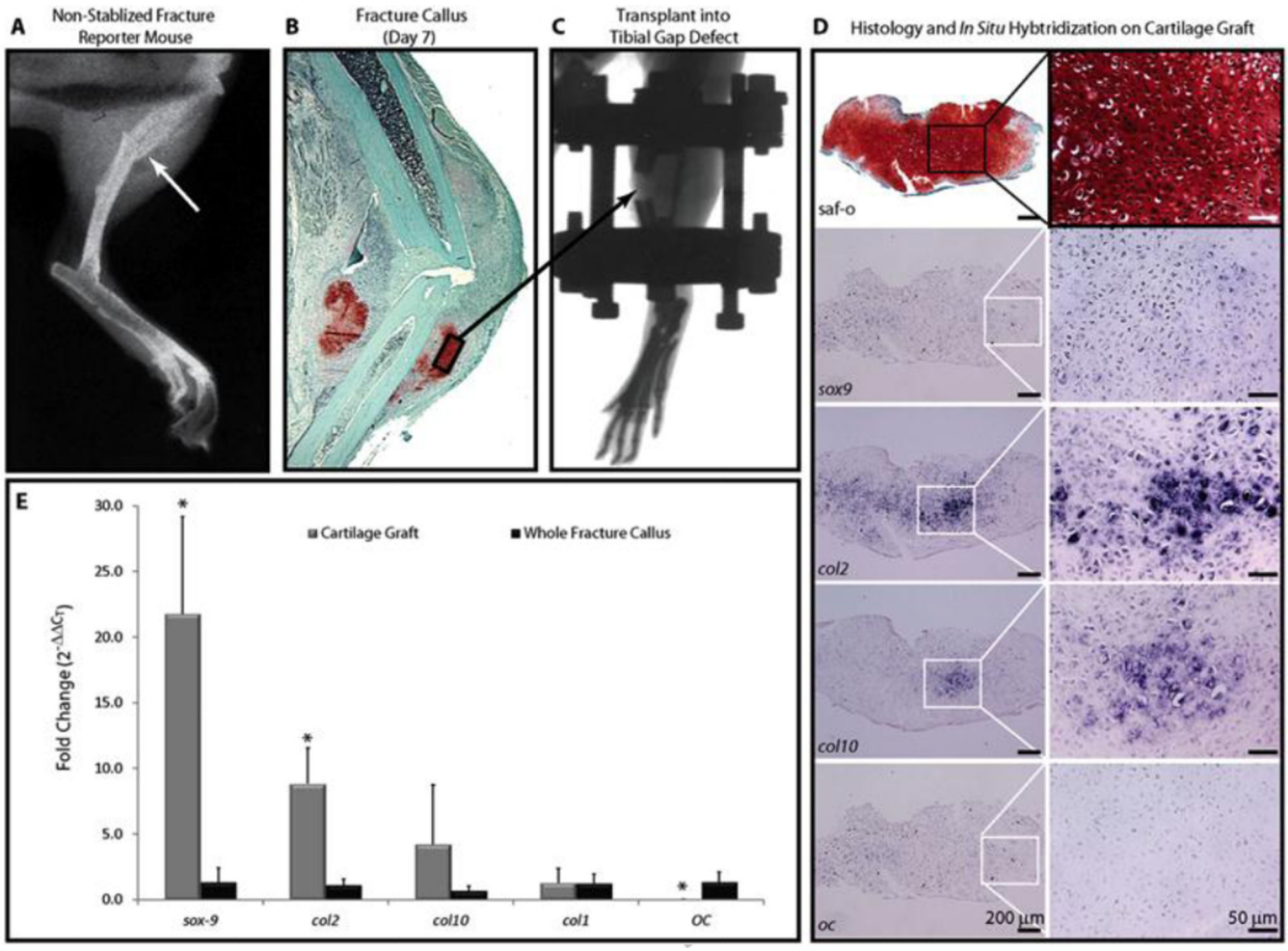

FIGURE 1. Cartilage Grafts from Fracture Callus

(A) X-ray image of unstabilized mid-diaphysial tibia fracture (arrow) created by three point bending. **(B)** Safranin-O staining of fracture callus 7 days following injury. Grafts were isolated *ex-vivo*, boxed region represents the approximate area from where grafts were harvested. **(C)** Grafts were transplanted into 2mm segmental defects created in the mid-diaphysis of externally stabilized murine tibia. **(D)** Safranin-O staining of the cartilage graft (top), followed by DIG-probe *in situ* hybridization for *sox-9, col2, col10, and osteocalcin (oc)*. **(E)** Quantitative RT-PCR shows gene expression in the cartilage graft (n=6) relative to the whole fracture callus (n=5), data represents mean ± 95% confidence, with significance (*) of $p < 0.005$.

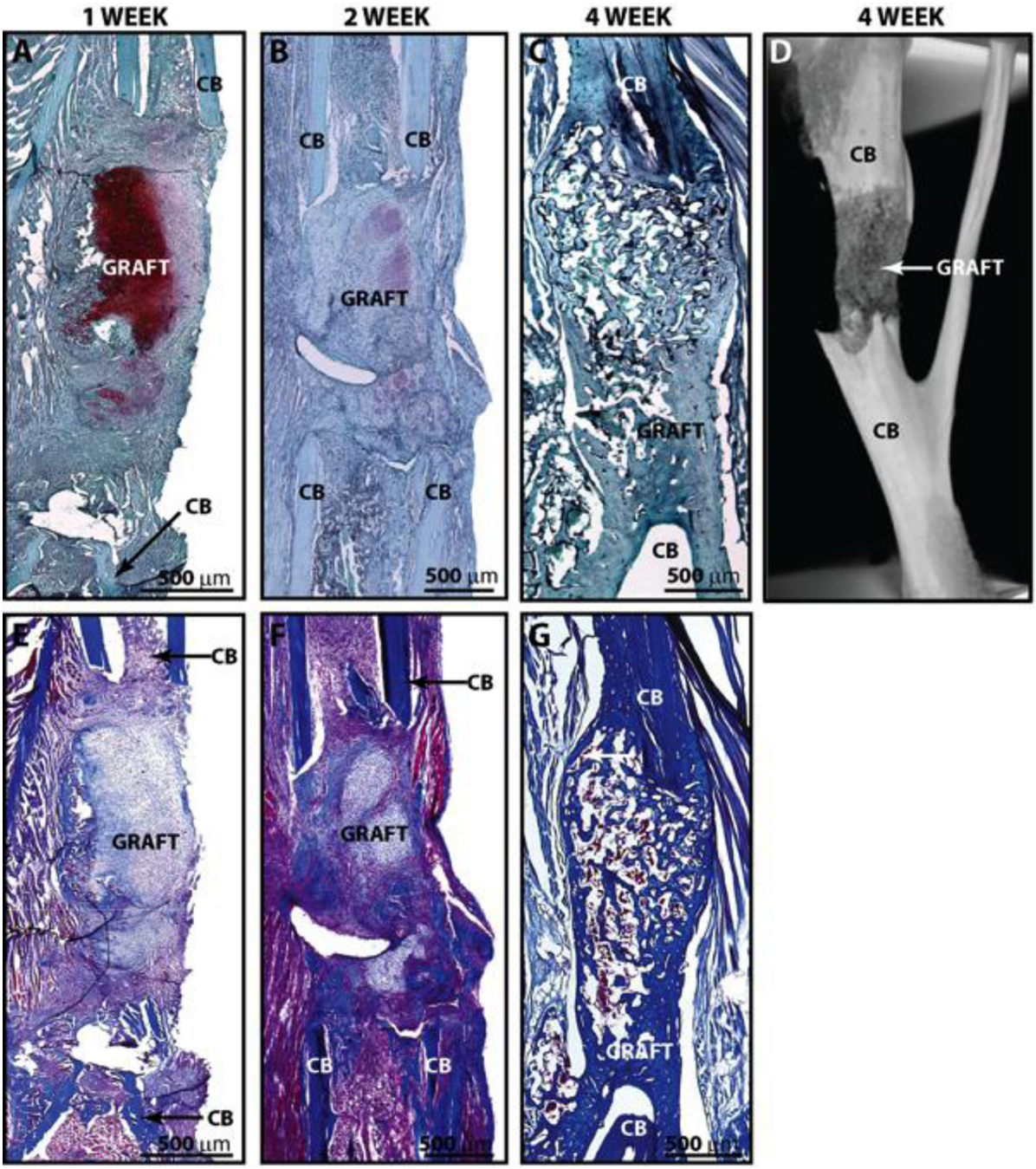

FIGURE 2. Cartilage grafts produce an integrated and vascularized bone regenerate in a segmental bone defect

(A–C) Safranin-O or **(E–G)** Masson's Trichrome staining at days **(A&E)** 7, **(B&F)** 14, or **(C&G–D)** 28 after implantation of the cartilage graft. **(D)** μCT image of tibia defect 4 weeks post-surgically. "cb" = cortical bone (host), "graft" = transplanted fracture callus cartilage.

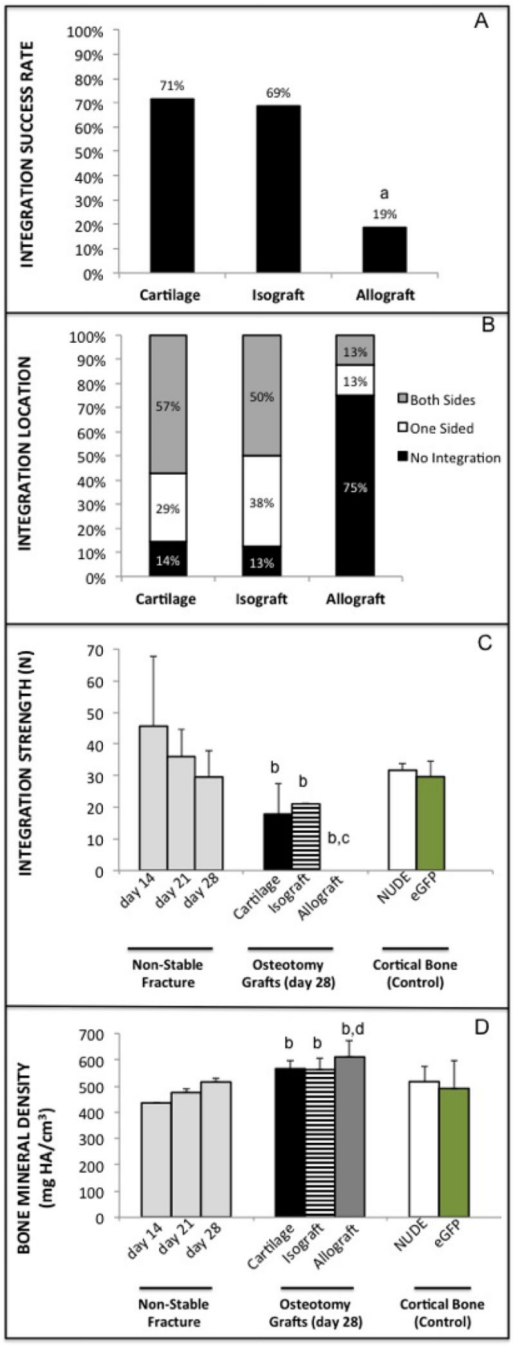

FIGURE 3. Integration of cartilage grafts is equivalent to isograft and superior to allograft after 4 weeks of healing

(A) Overall percentage that cartilage, isograft, or allograft integrated with the host tissue based on two potential integration sites per graft (7–8 animals, 14–16 integration opportunities; *a* = statistically different than cartilage and isograft, $p < 0.005$). **(B)** Graphical representation of integration for cartilage, isograft, and allograft. **(C)** Ultimate failure of grafts by three-point bending. Ultimate failure of uninjured cortical bone for both the grafts (eGFP) and host mice (immunocompromised/nude) are provided as a positive control

alongside failure of non-stabilized fractures for reference (*b* = statistically different than d14 fx, *c* = different than cortical bone, $P < 0.05$). **(D)** Bone mineral density (BMD) of the fracture callus, grafts and cortical bone (*d* = statistically different than d21 fx, $p < 0.02$).

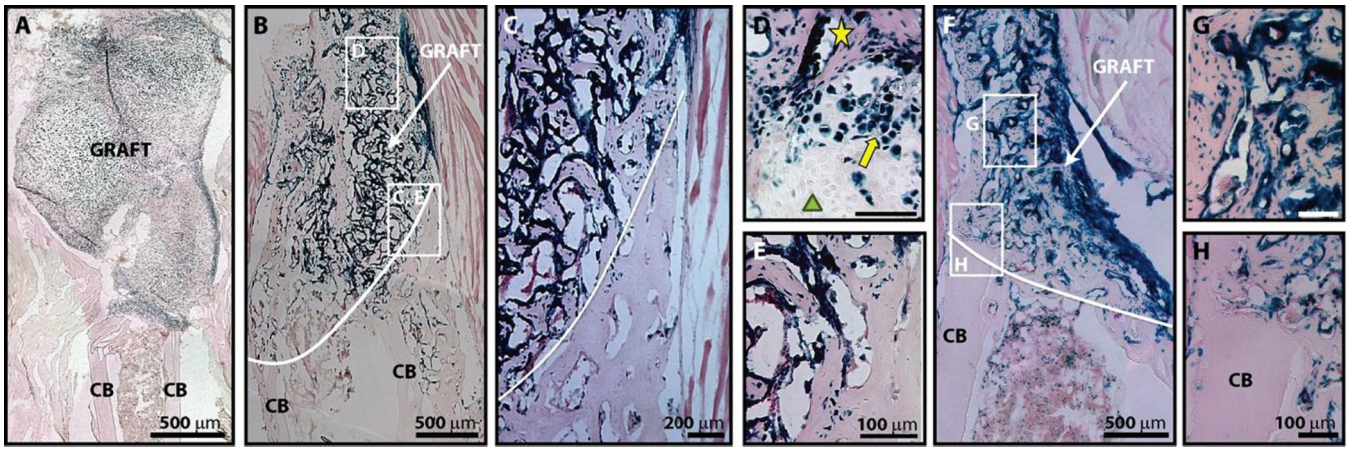

FIGURE 4. Donor (blue) versus host contribution to the bone regenerate

Cartilage grafts were obtained from Lac-$Z^{+/+}$-Rosa26 reporter mice and transplanted into immunocompromised mice (SCID Beige) mice. Donor cells were labeled using x-gal staining to detect β-galactosidase activity from the Rosa26 mice at **(A)** 7, **(B–E)** 28, or **(F–H)** 42 days after cartilage engraftment. Special characters **(D)** donor osteocytes (yellow star), donor chondrocytes (yellow arrow), host chondrocytes (green triangle). “cb” = cortical bone (host), “graft” = transplanted fracture callus cartilage from $LacZ^{+/+}$ mouse.

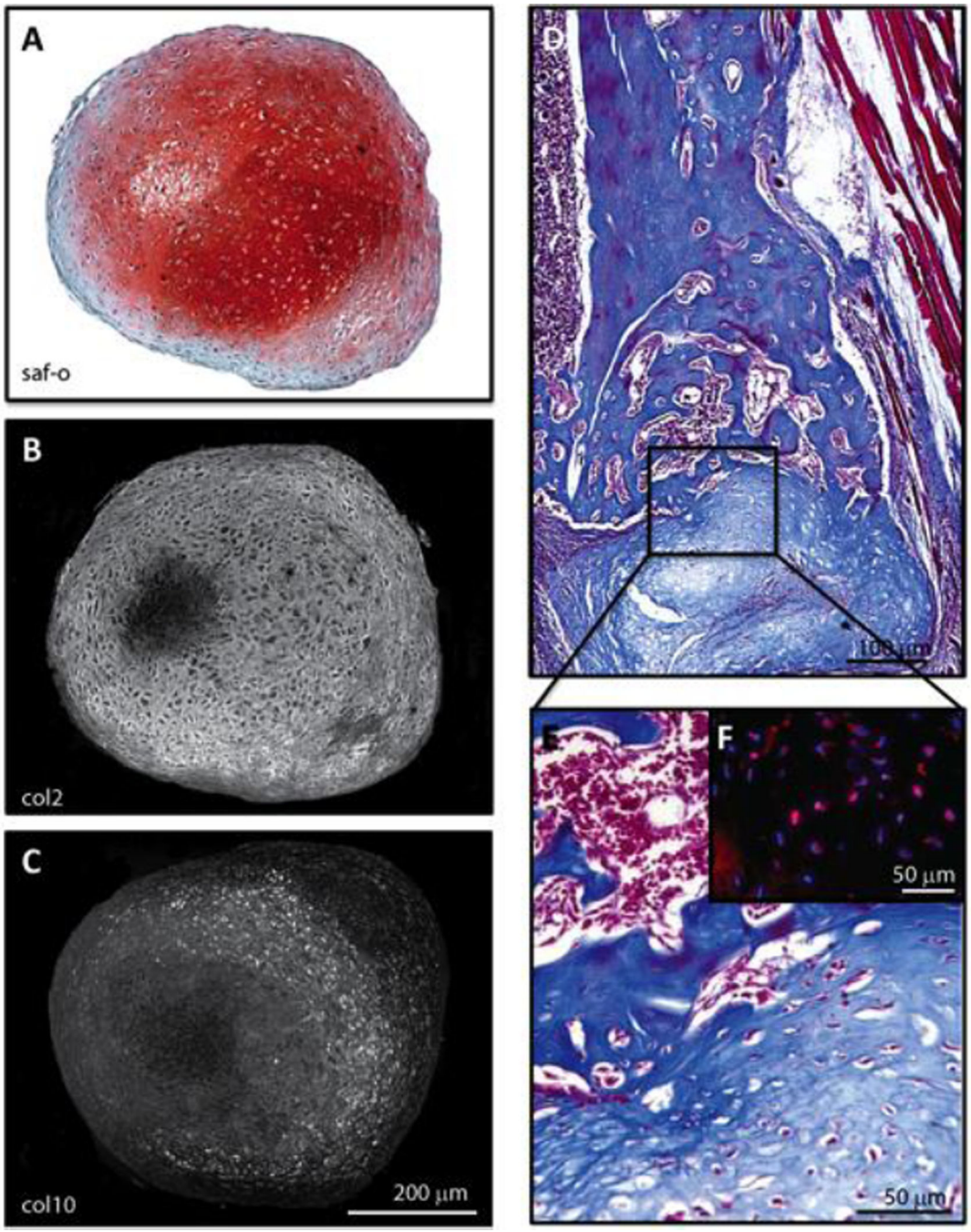

FIGURE 5. Human MSC-derived cartilage pellets transplanted into segmental bone defect regenerate bone

(A–C) hMSC pellets following 3 weeks of *in vitro* culture in chondrogenic conditions stained with **(A)** Safranin-O, or antibodies to **(B)** collagen II and **(C)** collagen X. **(D–E)** Masson's Trichrome staining of segmental defect 4 weeks following transplantation of hMSC-derived cartilage pellets. **(F)** hMSC-dervied pellet with antibody staining for human mitochondria in the trichrome positive bone.

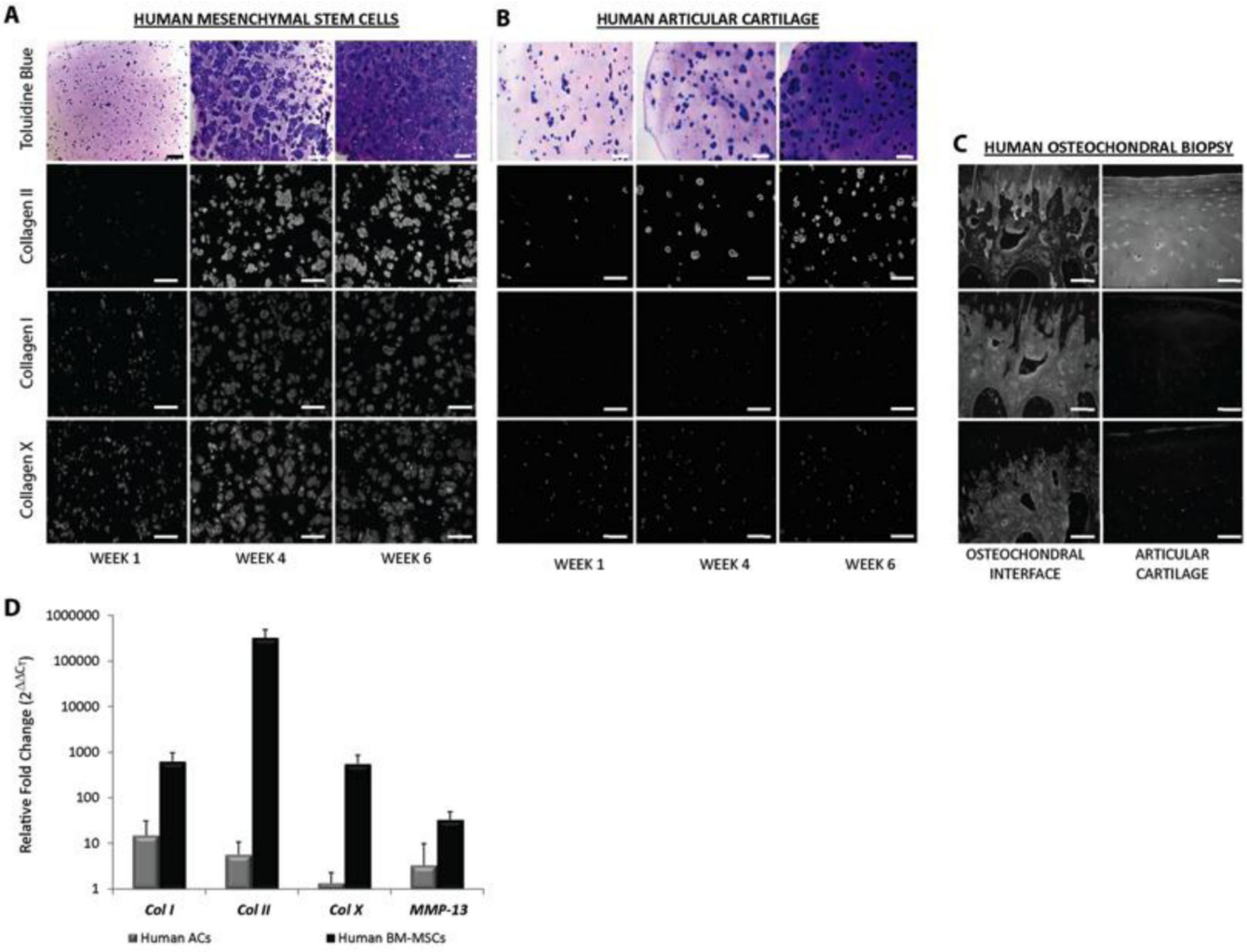

FIGURE 6. Engineering endochondral cartilage for tissue engineering

Human MSCs **(A)** or healthy human articular chondrocytes (hACs) **(B)** were photoencapsulated into PEGDA based scaffolds and cultured *in vitro* with chondrogenic medium for six weeks. **(C)** Antibody specificity was verified using articular cartilage and the osteochondral interface. **(D)** Gene expression of the hMSC (n=6) or hAC (n=6) derived tissue engineered cartilage following six weeks of *in vitro* culture was compared to gene expression of each tissue at day 0. Graph represents mean ± 95% confidence.

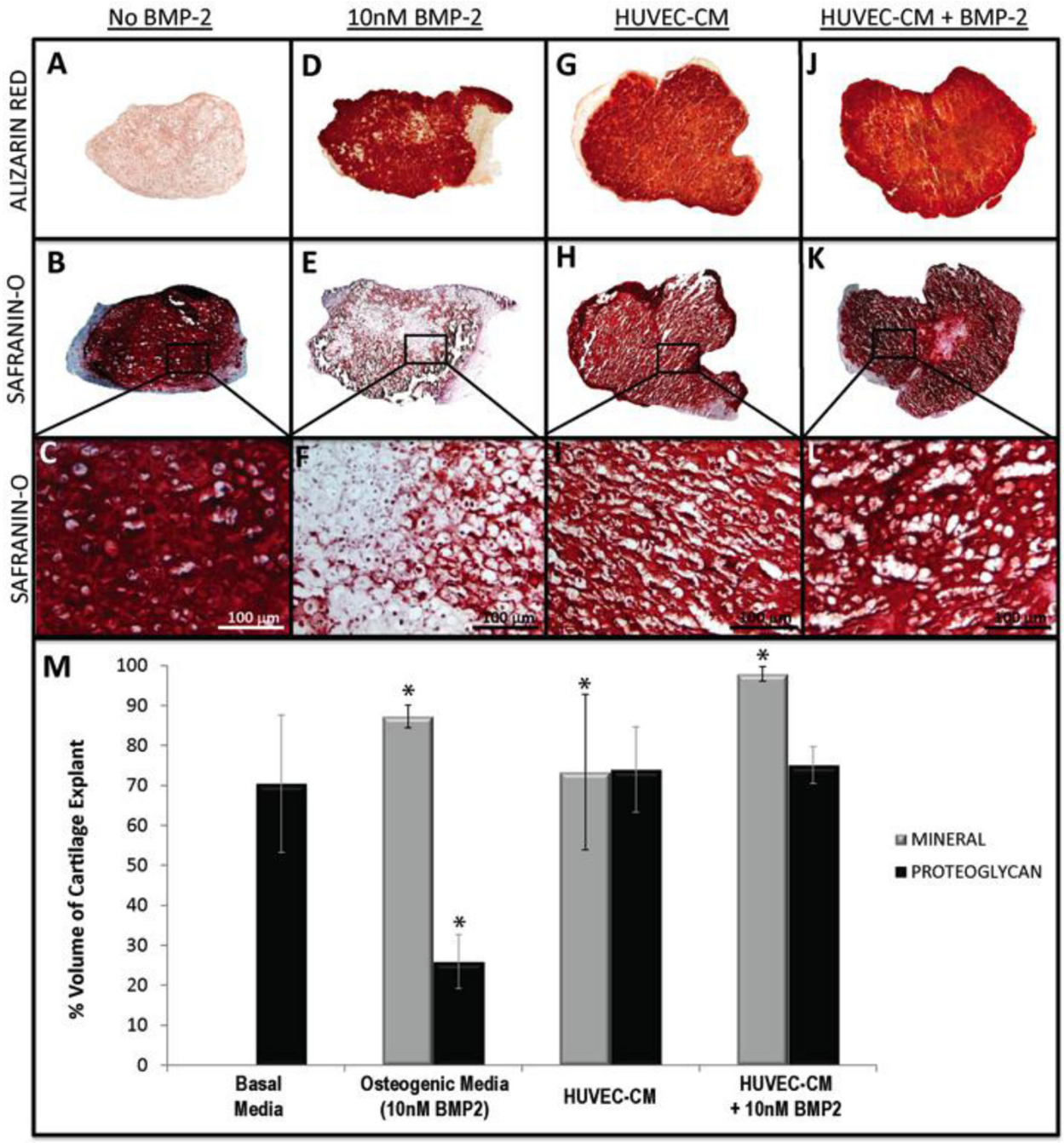

FIGURE 7. HUVEC conditioned medium is sufficient for producing mineralized cartilage *in vitro*

Alizarin red and safranin-o/fast green staining of cartilage obtained from the day-7 fracture callus and cultured *in vitro* in basal medium containing 10 nM dexamethasone and 100 μg/ml A2P for 2 weeks; then either maintained in that basal condition **(A–C)**, or transferred to osteogenic supplements (rhBMP2,βGP,A2P) **(D–F)**, HUVEC-CM **(G–I)**, or HUVEC-CM with osteogenic supplements **(J–L)**. Alizarin red and safranin-o/fast green staining of cartilage grafts **(M)**. Quantification of the percentage of mineralization (gray) and

proteoglycan (black) in cartilage explants following 4-weeks of *in vitro* culture. Graph represents mean ± 95% confidence, with significance (*) of $p < 0.005$.

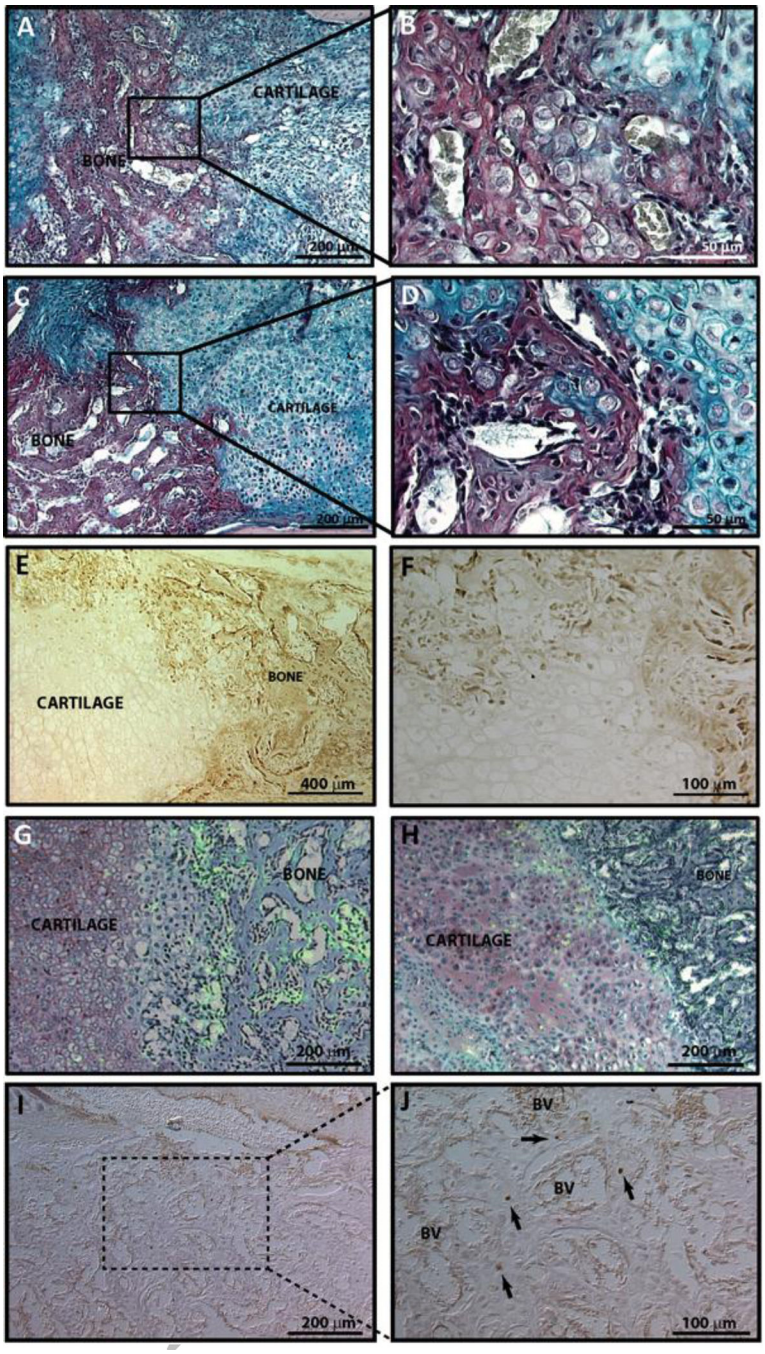

FIGURE 8. Cartilage to bone transition zone in fracture callus

(A–D) Hall and Brunt Quadruple stain (HBQ, bone = red, cartilage = blue) of non-stabilized fracture callus 10-days post-injury. **(E–F)** Osteocalcin immunohistochemistry of non-stabilized fracture callus 10-days post-injury. **(G–H)** *In situ* cell death detection (GFP) merged with Safranin-O (cartilage = red, bone = blue) staining of day **(G)** 7 or **(H)** day 10 fracture callus. **(I–J)** Oct4A immunohistochemistry of day 10 fracture callus. Arrows point to Oct4A positive hypertrophic chondrocytes, "BV" = blood vessel or bone marrow space.

TABLE 1

Primer Lists

Gene	Species	Syber Green	
		Forward	*Reverse*
GAPDH	mouse	TGATGACATCAAGAAGGTGGTGAAG	CCTTGGAGGCCATGTAGGCCAT
Sox9	mouse	GCAGACCAGTACCCGCATCT	CTCGTTCAGCAGCCTCCAG
Col2A	mouse	GGCTCCCAGAACATCACCTA	TCGGCCCTCATCTCTACATC
Col10A	mouse	AATCTGAAATGCAAGGTGCT	AAGACTCAAATAGTCATTAAAGCAAA
Col1A	mouse	CCCAGAACATCACCTATCAC	TTGGTCACGTTCAGTTGGTC
Osteocalcin	mouse	CGCTCTGTCTCTCTGACCTC	TCACAAGCAGGGTTAAGCTC

Gene	Species	Taqman Assay ID#
18S	human	hs9999999901_s1
ACAN	human	hs00153936_m1
Col2A	human	hs00264051_m1
Col10A	human	hs00166657_m1
Col1A	human	hs00164004_m1
MMP-13	human	Hs00233992_m1